Impedance Matrix Of An Antenna Array In A Quasi-Optical Resonator

Patrick L. Heron, Gregory P. Monahan, *Student Member, IEEE,* J. W. Mink, *Fellow, IEEE,* Felix K. Schwering, *Fellow IEEE,* and Michael B. Steer, *Senior Member, IEEE*

Abstract— **The power from numerous millimeter wave solid-state sources can be efficiently combined using quasi-optical techniques. One such technique is to place an array of active radiating sources within a quasi-optical resonator. The driving point impedance of each antenna is strongly affected by the presence of all other active antennas as well as by the mode structure and Q of the resonator. In this paper the impedance matrix for an array of antennas radiating into a plano-concave open resonator is determined through use of the Lorentz integral. The resulting expressions include the effect of diffraction loss and are valid for arbitrary reflector spacing, source frequency, array location and geometry. The result can be used to impedance match each active source to its antenna and thus facilitate design of an efficient power combining system. Simulations using the impedance matrix in conjunction with an antenna impedance model are compared with two-port measurements.**

I. Introduction

QUASI-OPTICAL techniques have been recognized as an attractive means for combining power from numerous solid-state millimeter-wave sources. Power combining is accomplished in free space through superposition of the fields produced by individual radiators which are either globally or locally phase locked. Quasi-optical power combiners have been constructed using a variety of active sources including MESFET's, IMPATT diodes, Gunn devices, and resonant tunneling diodes (RTD's). Various radiating elements have also been used including patch antennas, slot antennas, and open ended waveguide cavities. Several techniques are used to phase lock the individual oscillators, the locking being either global or local in nature. Combiners which lock oscillators through direct radiation from antennas are referred to as direct-radiation-coupled (DRC) combiners. Those which attain locking through the mode structure of a quasi-optical cavity are termed as being cavity- or resonator-coupled (RC) combiners. Both DRC and RC combiners utilize global coupling as each active element affects the driving point impedance of many other devices. The phase locking of RC combiners is more global in nature as the radiation from any one active device is distributed over the entire array of sources due to the resonator mode structure. The interaction in DRC combiners is greatest for nearest neighbors and the effect of one radiating element on the others is reduced with device separation. Circuit coupled (CC) power combiners achieve locking through microstrip transmission lines or other circuit elements. Such combiners are usually locally locked. Any of these combiner types can be self locking, or be injection locked by an external signal.

DRC combiners have the simplest structure, but the individual oscillators must be carefully designed to be nearly identical. This is necessary because the relatively weak field interaction between radiators results in a small oscillator locking bandwidth. Broadside radiation can be achieved with an in-phase oscillation regime, which is attained if the inter-radiator spacing is λ_0. This spacing results in grating lobes in the radiation pattern and also places constraints on the maximum area density of oscillators. The power combiner performance degrades if a single oscillating element fails due to the relatively local nature of the coupling. An example of a DRC combiner is that constructed and studied by Birkeland and Itoh [1]. Each active element was comprised of a patch antenna driven by two FET's locked in an odd oscillation mode by a microstrip line. Phase locking of four such oscillators by direct radiation coupling was attained. Very high combining efficiency was reported at 6 GHz. In general, the design theory and techniques used for array antennas can be applied to DRC combiner design.

CC combiners have a more complex structure than do DRC combiners because of additional coupling circuitry. The amount of coupling can be tailored by changing transmission line impedance or coupling circuit geometry, consequently the individual oscillator tolerances are not as critical. Inter-radiator spacing can be less than λ_0 depending upon the relative dielectric constant of the substrate so that the area density of oscillators can be higher than with DRC combiners. As with DRC combiners, performance suffers if a single element fails due to the local nature of the coupling.

Several researchers have constructed and analyzed CC power combiners which use microstrip transmission line coupling. Camilleri and Bayraktaroglu [2] have constructed and modeled a linear array of three oscillators at 43 GHz. Each oscillator was monolithically constructed and consisted of two IMPATT diodes and a resonant patch antenna. The use of multiple active devices for each oscillator allowed for an increased device area density. Mortazawi and Itoh [3] designed and constructed an X-band second harmonic quasi-optical power combiner. Four X-band Gun diode oscillators

Manuscript received August 18, 1992; revised March 30, 1992.

This work was supported in part by the U.S. Army Research Office through grant DAAL03-89-G-0030.

P. L. Heron, G. P. Monahan and M. B. Steer are with the High Frequency Electronics Laboratory, Department of Electrical and Computer Engineering, North Carolina State University, Raleigh, 27695-7911

J. W. Mink is with the United States Army Research Office, P.O. Box 12211, Research Triangle Park, NC 27709-2211. F. K. Schwering is with CECOM, Attn. AMSEO-RD-C3-ST, Ft. Monmouth, NJ 07703-5203.

IEEE Log Number 9211915.

were placed periodically along a microstrip transmission line. Each oscillator was carefully designed to produce high levels of second harmonic output and had an associated patch antenna that was resonant at the second harmonic frequency. Thus the oscillators were phase locked at the fundamental frequency through the transmission line, but radiated at the second harmonic frequency.

Birkeland and Itoh [4] have constructed a CC quasi-optical power combiner using MESFET's. Each element consisted of a two port FET oscillator and a patch antenna which was phase locked by use of microstrip couplers. A five element linear array operating at 6 GHz was constructed. The first oscillator in the chain was fed by an external locking signal while successive oscillators picked up their respective injection signals from the output port of the previous oscillator in the chain. Coupling via radiation was avoided by use of a non-planar structure to isolate the coupling structures from the radiators. Circuit coupled combiners can be analyzed and designed using existing simulators for planar microwave circuit analysis.

RC and DRC quasi-optical combiners use similar planar circuits. The added resonant cavity of the RC combiner requires precise control of dector spacing and curvature. There are, however, several advantages to using resonator coupling. Due to the resonator mode structure, inter-element spacing is arbitrary thus oscillator element density can be maximized. Phase locking is truly global in nature which can result in relative immunity of combiner performance to device failure. Furthermore, the strong field levels inside the cavity allow for the use of more compact sub-resonant antennas. The cavity field interactions also result in larger locking bandwidth, thus the individual oscillator tolerance can be relaxed as compared with a DRC scheme. Open resonators can produce a highly focused radiation pattern. York and Compton [5] have observed improved performance of a DRC power combiner when placed in a low Q cavity.

Popović et al. [6] have constructed and modeled a 10×10 MESFET planar grid RC power combiner. The MESFET's were located at the intersections of a regular grid of conductors (of pitch $\lambda_0/8$) which was supported by a dielectric substrate. A planar metallic reflector was placed beneath the dielectric so that the grid and planar reflector formed an open resonator. The characteristics of the unloaded grid were measured quasi-optically and fit to a circuit model for a grid unit cell. Derivation of the unit cell model required the assumptions that the array was infinite and that all MESFET's were identical. The frequency of oscillation was predicted, but output power was not.

Mink [7] has studied an array of filamentary current sources radiating into a plano-concave open resonator. This was the first theoretical investigation of power combining using a source array in a quasi-optical resonator. The results are applicable to the design of RC quasi-optical combiners and were obtained by use of the Lorentz reciprocity theorem to find the coupling coefficients between the current elements and the natural short-circuit modes of the cavity. The mode coupling coefficients and the radiation resistance were determined for equal and Gaussian weighted sources under that assumption that all modes resonated at a single frequency and that the resonator Q was high. Xue and Wang [8] have used Mink's result to study the effects of the longitudinal location of the source array in an open cavity. Wang *et al.* [9] went further to obtain the source spacing required in the transverse plane to optimize either the fundamental mode power, or the combining efficiency for an array of small current elements.

Antenna array theory and planar circuit theory may be used to design DRC and CC type power combiners. The objective of this paper is to derive a circuit level model based upon field calculations for an antenna array radiating into a plano-concave resonator. RC power combiner design can then be accomplished by using the model in conjunction with a simulator that is capable of modeling active devices and performing oscillator analysis. In this paper the source array impedance is determined by employing the same techniques used by Mink. The method of analysis is extended to calculate complex impedance for operation at arbitrary frequency and resonator spacing and is also valid for cavities having increased output power coupling. A specific resonator type and antenna configuration is considered here, but the concepts are applicable in general.

The quasi-optical resonator model is derived in sections II-IV by application of the Lorentz integral to determine the coupling coefficients which relate array element current to the resonator short circuit fields. The field structure is defined to include off-resonance operation. A reaction principle and knowledge of the coupling coefficients are used to determine an expression for the array impedance matrix. The resulting equations is applied to short thin-wire antennas to obtain simplified equations. In Section V the behavior of the simplified equations are compared with two port impedance measurements of antennas radiating into the cavity. While the formulae that are used pertain only to short antennas, the method is valid for arbitrary antenna geometry.

II. Combiner Configuration and Field Structure

The power combiner configuration considered here is similar to that studied by Mink [7]. The configuration is shown in Fig. 1 and consists of an array of current elements located at $z = d$, within a transverse $(x-y)$ plane of a plano-concave open resonator. The current elements represent small dipoles which are assumed to be driven by active devices. The resonator provides a high Q impedance which allows the individual elements to oscillate at specific frequencies. The oscillating elements are phase locked through the resonator mode structure which accomplishes the power combining. The resonator consists of an infinite, perfectly conducting plane located at $z = 0$, and partially transparent, spherical reflector having rectangular boundaries which is located at $z = D$. The field structure in similar resonators has been studied extensively during microwave maser research [10]–[16]. We will consider the fields to be a superposition of linearly polarized wave beam modes traveling in the $+\hat{a}_z$ direction, and in the $-\hat{a}_z$ direction. The beam modes, which are solutions to the paraxial wave equation, were described by Goubau and Schwering [17]. It is assumed that the fields in the res-

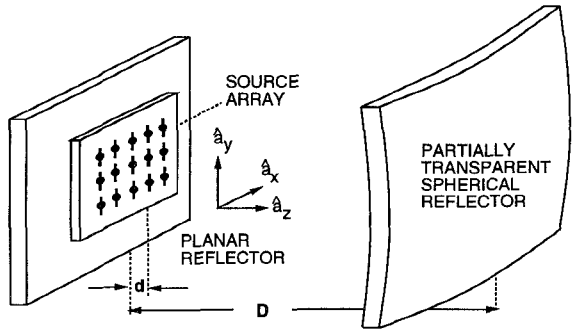

Fig. 1. Quasi-optical power combiner configuration.

onator have small divergence from propagation parallel to the z-axis, the paraxial condition. This condition can be enforced by appropriate system design. The eigen-functions can then be approximated by the product of Laguerre polynomials with Gaussian functions if polar coordinates are used in the transverse plane, or Hermite polynomials and Gaussian functions if rectangular coordinates are used in the transverse plane [10], [17]. If the paraxial condition is violated, then spheroidal wave functions in the prolate spheroidal coordinate system must be used [10]. The results of this paper can be modified for alternate resonator geometries by substituting the eigenfunctions appropriate for the particular geometry. Energy is coupled out of the power combiner by transmission through the spherical reflector.

In this work the following definition of the Hermite polynomials is used:

$$He_n(X) = (-1)^n \exp(X^2/2) \frac{d^n}{dX^n} \left(\exp(-X^2/2)\right). \quad (1)$$

These polynomials form a complete set and satisfy the orthogonality condition

$$\int_{-\infty}^{+\infty} He_s(X) He_m(X) w(X)\, dX = m!\, \delta_{sm} \sqrt{2\pi} \quad (2)$$

where the weight function $w(X) = \exp(-X^2/2)$, and δ_{sm} is the Kronecker delta. The linearly polarized wave beam modes form a complete, ortho-normal system [16] and each E-field mode can be written as

$$\begin{aligned} E^{\pm}_{mn}(x,y,z) = {} & \frac{(\mu/\epsilon)^{1/4}}{\sqrt{\pi \bar{X} \bar{Y} m!\, n!}} \left(1+u^2\right)^{-1/4} \\ & \cdot \left(1+v^2\right)^{-1/4} He_m\left(\sqrt{2}x/x_z\right) He_n\left(\sqrt{2}y/y_z\right) \\ & \cdot \exp\left\{ -\frac{1}{2}\left[(x/x_z)^2 + (y/y_z)^2\right] \mp j \right. \\ & \cdot \left[kz + \frac{1}{2}\left(u(x/x_z)^2 + v(y/y_z)^2\right) \right. \\ & - \left(m+\frac{1}{2}\right) \tan^{-1}(u) \\ & \left. \left. - \left(n+\frac{1}{2}\right) \tan^{-1}(v) \right] \right\}. \end{aligned} \quad (3)$$

For wave beams propagating in the $\pm\hat{a}_z$ direction, the H-field is related to the E-field by

$$\boldsymbol{H}^{\pm}_{mn} = \pm \sqrt{\frac{\epsilon}{\mu}}\, \hat{a}_z \times \boldsymbol{E}^{\pm}_{mn} \quad (4)$$

where,

$$u = \frac{z}{k\bar{X}^2}, \qquad v = \frac{z}{k\bar{Y}^2}$$
$$x_z^2 = \bar{X}^2\left(1+u^2\right), \qquad y_z^2 = \bar{Y}^2\left(1+v^2\right).$$

The E^+ and H^+ field components correspond to Gaussian wave beams which are diverging from a beam waist at $z = 0$ and traveling in the $+\hat{a}_z$ direction. The E^- and H^- terms are fields converging toward the beam waist while traveling in the $-\bar{a}_z$ direction. In each transverse plane the Gaussian envelope of the field strength decays with the form $\exp(-cr^2)$ from a maximum value at the origin, $x, y = 0$. The variables $\bar{X}$ and $\bar{Y}$ are called the Gaussian mode parameters and determine this rate of field strength decay in the x and y directions respectively. The mode parameters are found as [16]

$$\bar{X}^2 = \frac{1}{k}\sqrt{\left(F_x D\left(2 - \frac{D}{F_x}\right)\right)},$$

$$\bar{Y}^2 = \frac{1}{k}\sqrt{\left(F_y D\left(2 - \frac{D}{F_y}\right)\right)}$$

where k is the free space number and F_x, F_y are the focal lengths of the concave reflector due to curvature along the x and y axes respectively. From (2), (3), and (4) we can see that the wave beam modes satisfy an orthogonality condition in any transverse plane S,

$$\int_S \boldsymbol{E}^{\pm}_{st} \times (\boldsymbol{H}^{\pm}_{mn})^* \cdot \hat{a}_z\, dS = \mp \delta_{sm}\delta_{tn}. \quad (5)$$

For these linearly polarized modes we have adopted the convention

$$\boldsymbol{E}^{\pm}_{mn} = \pm \hat{a}_x E^{\pm}_{mn}; \qquad \boldsymbol{H}^{\pm}_{mn} = \hat{a}_y H^{\pm}_{mn}. \quad (6)$$

The relationship between the "forward" and "backward" traveling wave beams within the resonator can be found by specifying the properties of the spherical reflector. Each beam mode is referenced to a beam waist at $z = 0$, and the power carried by a beam mode is constant through any transverse plane. This allows us to formulate scattering parameters for the transverse fields. The reflector is characterized as a reciprocal lossless two-port element for Gaussian beams. The scattering parameters for such a junction are [18]

$$S_{11} = S_{22} = R_{mn} \quad (7)$$

and

$$\begin{aligned} S_{12} = S_{21} &= T_{mn} \\ &= \sqrt{1 - |R_{mn}|^2}\, \exp\left(j\left(\arg(R_{mn}) + \frac{\pi}{2} + h\pi\right)\right). \end{aligned} \quad (8)$$

for some integer h.

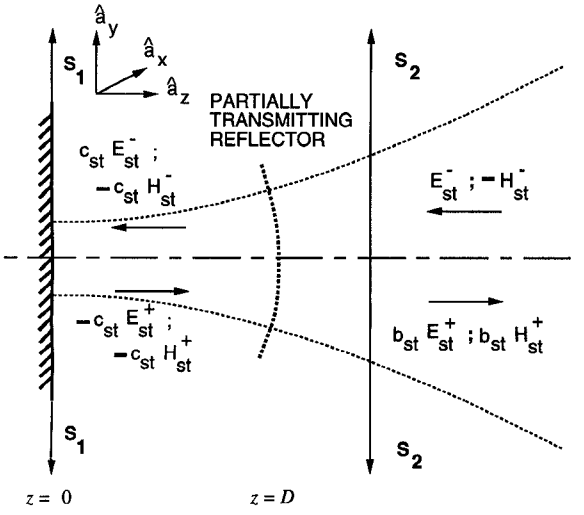

Fig. 2. Cross-section of quasi-optical resonator showing test fields, $\boldsymbol{E}_1$.

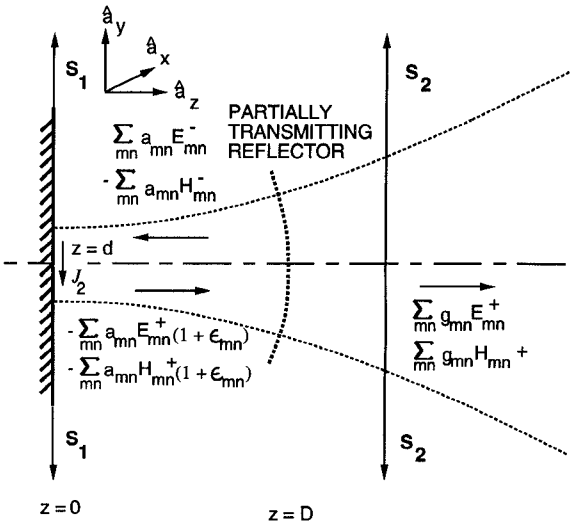

Fig. 3. Cross-section of quasi-optical resonator showing fields, $\boldsymbol{E}_2$, established by radiating current elements.

III. Application of Lorentz Reciprocity Theorem

Here the Lorentz reciprocity theorem is applied to determine the coefficients which describe coupling between an array of current elements and the resonator modal fields. Integration is evaluated for the volume enclosed by two infinite planar surfaces; S_1, the perfectly conducting plane reflector located at $z = 0$, and S_2, an infinite transverse plane located outside the resonator at $z > D$. For application of the Lorentz integral, the assumed forms of a test field and the field excited by the current array must be specified.

The test field is excited by a unit-amplitude, single-mode wave beam which originates from $z \gg D$ and converges upon the resonator, see Fig. 2. The incident beam excites a single resonator mode, as well as a modal beam traveling in the $+\hat{\boldsymbol{a}}_z$ direction for $z > D$. The fields inside the resonator, which are excited by the incident beam, consist of a wave beam $c_{st}\boldsymbol{E}^-_{st}$ traveling in the $-\hat{\boldsymbol{a}}_z$ direction, and a beam $\acute{c}_{st}\boldsymbol{E}^+_{st}$ traveling in the $+\hat{\boldsymbol{a}}_z$ direction. Since S_1 is a perfect conductor, we can apply the boundary condition $\hat{\boldsymbol{a}}_z \times \left(c_{st}\boldsymbol{E}^-_{st} + \acute{c}_{st}\boldsymbol{E}^+_{st}\right) = 0$ at $z = 0$, and find that $\acute{c}_{st} = -c_{st}$. Thus the test field, denoted $\boldsymbol{E}_{1,et}$, is

$$\boldsymbol{E}_{1,st} = \hat{\boldsymbol{a}}_x \begin{cases} c_{st}\left(E^-_{st} - E^+_{st}\right); & 0 < z < D \\ \left(E^-_{st} + b_{st}E^+_{st}\right); & z > D \end{cases}, \tag{9}$$

and $\boldsymbol{H}_{1,st}$ is found using (4). The field $0 < z < D$ is a standing wave and is commonly referred to as the TEM_{mnq} resonator mode. The subscripts m and n refer to the transverse mode order along the x- and y-axes, and q is the longitudinal mode number which will not be stated explicitly.

The properties of the spherical reflector can be used to determine the coefficients c_{st} and b_{st}. Using the transmission and reflection coefficients at the reflector surfaces yields

$$c_{st}E^-_{st} = T_{st}E^-_{st} - c_{st}R_{st}E^+_{st}$$

and,

$$b_{st}E^+_{st} = R_{st}E^-_{st} - c_{st}T_{st}E^+_{st}.$$

Solving for c_{st} and b_{st}

$$c_{st} = \frac{T_{st}}{1 + R_{st}\psi_{st}} \tag{10}$$

and,

$$b_{st} = \frac{R_{st}}{\psi_{st}} - \frac{T^2_{st}}{1 + R_{st}\psi_{st}}. \tag{11}$$

where $\psi_{st} \equiv E^+_{D,st}/E^-_{D,st}$, and the notation $E^{\pm}_{D,st}$ is used to indicate $E^{\pm}_{st}$ evaluated on the surface of the spherical reflector. Since the phase fronts of all traveling beam modes correspond approximately to the surface of the spherical reflector [15], during calculations we will evaluate ψ_{st} at $\{x, y, z\} = \{0, 0, D\}$.

The fields, $\boldsymbol{E}_2$ and $\boldsymbol{H}_2$ are excited by an array of $\hat{\boldsymbol{a}}_x$ directed current sources $\boldsymbol{J}_2$ as shown in Fig. 3. Since the beam modes form a complete ortho-normal set, we can expand these source fields in terms of beam modes. The magnetic field is found from the electric field using (4), and the linearly polarized electric field is

$$\boldsymbol{E}_2 = \hat{\boldsymbol{a}}_x \sum_{mn} \begin{cases} f_{mn}(E^-_{mn} - E^+_{mn}); & 0 \le z < d \\ a_{mn}(E^-_{mn} - (1+\varepsilon_{mn})E^+_{mn}); & d < z \le D \\ g_{mn}E^+_{mn}; & z > D \end{cases}. \tag{12}$$

The field in the region $0 \le z < d$ is a standing wave due to the perfectly conducting plane S_1. The resonator field for $d < z \le D$ is comprised of a standing wave and a traveling wave. The traveling wave component has amplitude $a_{mn}\varepsilon_{mn}$ which corresponds to power transmission through the curved reflector. The field for $z > D$ carries the useful output power. The reflector characteristics described by (7) and (8) are again applied along with (12) to find

$$\varepsilon_{mn} = -\frac{1}{\psi_{mn}R_{mn}} - 1 \tag{13}$$

and

$$a_{mn} = \frac{g_{mn}\psi_{mn}R_{mn}}{T_{mn}}. \tag{14}$$

The source fields in the region $0 \leq z < d$ can be related to the fields in the region $d < z \leq D$ if we assume continuity of the electric field on a mode by mode basis at the plane $z = d$. Equating the modal fields at $z = d$ we get

$$f_{mn} = a_{mn} \frac{(1 + \Upsilon_{mn}/(R_{mn}\psi_{mn}))}{(1 - \Upsilon_{mn})}. \tag{15}$$

Where the ratio $\Upsilon_{mn} \equiv E^+_{mn}/E^-_{mn}$ is evaluated at $x, y, z = 0, 0, d$. Near the surface $z = 0$ the phase fronts of E^+_{mn} and E^-_{mn} are nearly planar so for fixed z, Υ_{mn} is approximately independent of x and y.

The reciprocity theorem is now applied over the volume bounded by $S = S_1 + S_2$ to find the relationship between $\boldsymbol{J}_2$ and g_{mn}.

$$\oint_S (\boldsymbol{E}_1 \times \boldsymbol{H}_2 - \boldsymbol{E}_2 \times \boldsymbol{H}_1) \cdot \hat{\boldsymbol{n}}\, dS = -\int_V \boldsymbol{E}_1 \cdot \boldsymbol{J}_2\, dV. \tag{16}$$

The surface integral vanishes on S_1, because it is a perfect conductor, then using (9) and (12) the left hand side of (16) can be written as

$$\sum_{mn} g_{mn} \int_{S_2} (\boldsymbol{E}^-_{st} \times \boldsymbol{H}^+_{mn} + b_{st}\boldsymbol{E}^+_{st} \times \boldsymbol{H}^+_{mn} - \boldsymbol{E}^+_{mn} \times \boldsymbol{H}^-_{st} - b_{st}\boldsymbol{E}^+_{mn} \times \boldsymbol{H}^+_{st}) \cdot \hat{\boldsymbol{a}}_z\, dS. \tag{17}$$

Consider the quantity $\boldsymbol{E}^+_{st} \times \boldsymbol{H}^+_{mn}$ in the second term of (17). Using (4) this term becomes

$$\begin{aligned} \boldsymbol{E}^+_{st} \times \boldsymbol{H}^+_{mn} &= \left\{-\sqrt{\frac{\mu}{\epsilon}}\hat{\boldsymbol{a}}_z \times \boldsymbol{H}^+_{st}\right\} \times \left\{\sqrt{\frac{\epsilon}{\mu}}\hat{\boldsymbol{a}}_z \times \boldsymbol{E}^+_{mn}\right\} \\ &= \{-\hat{\boldsymbol{a}}_z \times \hat{\boldsymbol{a}}_y \boldsymbol{H}^+_{st}\} \times \{\hat{\boldsymbol{a}}_z \times \hat{\boldsymbol{a}}_x E^+_{mn}\} \\ &= E^+_{mn} H^+_{st} \{\hat{\boldsymbol{a}}_x \times \hat{\boldsymbol{a}}_y\} \\ &= E^+_{mn} H^+_{st} \hat{\boldsymbol{a}}_z = \boldsymbol{E}^+_{mn} \times \boldsymbol{H}^+_{st}, \end{aligned} \tag{18}$$

so that the second and fourth terms in (17) cancel. Now applying the orthogonality condition (5) to the two remaining terms of (17), and using (9), (10) on the right hand side of (16), the reciprocity relationship becomes,

$$2g_{mn} = \frac{-T_{mn}}{1 + R_{mn}\psi_{mn}} \int_V (E^-_{mn} - E^+_{mn}) \hat{\boldsymbol{a}}_x \cdot \boldsymbol{J}_2\, dV. \tag{19}$$

This result relates the modal source fields to the current of the array elements. The expression (19) assumes that $\boldsymbol{E} = \hat{\boldsymbol{a}}_x E$ and thus $\boldsymbol{J}_2 = \hat{\boldsymbol{a}}_x J_2$. For a general $\boldsymbol{J}_2$ confined to a transverse plane, an $\hat{\boldsymbol{a}}_y$ polarization term for E must be included in (12) and (9). The calculation of (16) then proceeds as before.

IV. Source Array Impedance Matrix

A. Impedance

It is desirable to model the resonator and antenna array as a linear multiport circuit for purposes of quasi-optical power combiner analysis and design. Each port of the circuit corresponds to the terminals of a particular antenna. An active element can be placed at each port to construct a power combiner. Due to the nonlinear nature of the active devices, a computer simulator would then be used for analysis. An expression will be determined for the impedance matrix of an array of infinitesimal dipole antennas each aligned in the $\hat{\boldsymbol{a}}_x$ direction with the pth antenna located at $x, y, z = \{x_p, y_p, z_p\}$. It is assumed that the dipoles are short enough that the resonator modal fields do not vary appreciably over their length. This assumption is reasonable for non-resonant antennas because a consequence of the paraxial condition is that the field strength must vary slowly in the transverse plane as compared with the axial field strength variations. For this array, (19) takes the very simple form

$$2g_{mn} = \frac{-T_{mn}}{(1 + R_{mn}\psi_{mn})} \sum_q I_q \Delta X_q (E^-_{q,mn} - E^+_{q,mn}). \tag{20}$$

Where $E^{\pm}_{q,mn}$ is $E^{\pm}_{mn}$ evaluated at $\{x_q, y_q, z_q\}$, and I_q and ΔX_q are the terminal current and effective length of the qth dipole respectively.

The driving point impedance of the pth dipole in the presence of all other dipoles is found by use of a reaction principle [19]

$$Z_p = -\frac{1}{I_p^2} \int_V \boldsymbol{J}_p \cdot \boldsymbol{E}_2\, dV. \tag{21}$$

Next using the field expansion (12), with the expansion coefficients given by (14), (15) and (20) along with the short dipole approximation, the driving point impedance of the pth dipole in the presence of the other dipoles is

$$Z_p = \frac{\Delta X_p}{2I_p} \sum_{mn} \cdot \left[\frac{(R_{mnn}\psi_{mn} + \Upsilon_{mn})}{(1 + R_{mn}\psi_{mn})(1 - \Upsilon_{mn})} \cdot (E^-_{p\,mn} - E^+_{p\,mn}) \sum_q I_q \Delta X_q (E^-_{q,mn} - E^+_{q,mn})\right] \tag{22}$$

To characterize the array, we seek the elements z_{pq} of the impedance matrix Z which satisfies the equation

$$\boldsymbol{V} = \boldsymbol{Z}\boldsymbol{I} \tag{23}$$

where $\boldsymbol{V}/\boldsymbol{I}$ are vectors of antenna terminal voltages/currents.

The elements, z_{pq}, of the impedance matrix $\boldsymbol{Z}$ must be found but we cannot directly set $I_p = 0$ in (22). Consider one of he equations obtained from (23) by setting all $I = 0$ except $I_p = I_q = \hat{I}$. Thus

$$v_p = z_{pp} I_p + z_{pq} I_q = (z_{pp} + z_{pq})\hat{I}$$

so that

$$z_{pp} + z_{pq} = \frac{v_p}{\hat{I}}.$$

For this linear device, the driving point impedance with two active sources is the sum of the impedances when the same sources act individually. Any desired value for I_p and I_q may be chosen because z_{pp} and z_{pq} are independent of the values

of these currents. Thus $z_{pp}+z_{pq}$ is found from (22) by setting $I=0$ except $I_p=I_q=\hat{I}$.

$$z_{pp}+z_{pq}=\frac{\Delta X_p}{2}\sum_{mn}\Bigg[\frac{(R_{mn}\psi_{mn}+\Upsilon_{mn})}{(1+R_{mn}\psi_{mn})(1-\Upsilon_{mn})}\cdot\left(E^-_{p,mn}-E^+_{p,mn}\right)\cdot\left(\Delta X_q\left(E^-_{q,mn}-E^+_{q,mn}\right)+\Delta X_p\left(E^-_{p,mn}-E^+_{p,mn}\right)\right)\Bigg]. \tag{24}$$

Subtracting z_{pp} from (24) yields z_{pq}. The diagonal term, z_{pp}, is found from (22) by setting all $I_q=0$ for $q\neq p$. When the expression for z_{pp} is subtracted from (24), the general impedance matrix term is found to be

$$z_{pq}=\frac{\Delta X_p\Delta X_q}{2}\sum_{mn}\Bigg[\frac{(R_{mn}\psi_{mn}+\Upsilon_{mn})}{(1+R_{mn}\psi_{mn})(1-\Upsilon_{mn})}\cdot\left(E^-_{p,mn}-E^+_{p,mn}\right)\cdot\left(E^-_{q,mn}-E^+_{q,mn}\right)\Bigg]. \tag{25}$$

Alternatively, the expression for z_{pq} can also be derived by finding E_2 when I_q acts along, then using $z_{pq}=v_{pq}/I_q$, where

$$v_{pq}=-\int \boldsymbol{E}_2\cdot\hat{\boldsymbol{d}}\ell_p=-\Delta X_p E_{p,2}\,.$$

The result, (25), applies to infinitesimal $\hat{\boldsymbol{a}}_x$-directed current sources. If both field polarizations are included and the small antenna assumption is removed, using (21) as the definition of impedance, (22) becomes

$$Z_p=\frac{1}{2I_p^2}\sum_{mn}\frac{(R_{mn}\psi_{mn}+\Upsilon_{mn})}{(1+R_{mn}\psi_{mn})(1-\Upsilon_{mn})}\cdot\int_V\left(E^-_{mn}-E^+_{mn}\right)J_p\cdot\int_{\acute{V}}\left(\acute{E}^-_{mn}-\acute{E}^+_{mn}\right)\cdot\left(\hat{\boldsymbol{a}}_x\hat{\boldsymbol{a}}'_x+\hat{\boldsymbol{a}}_y\hat{\boldsymbol{a}}'_y\right)\cdot\boldsymbol{J}'_2\,dV'\,dV \tag{26}$$

where $\boldsymbol{J}_p$ is the source current density on the pth antenna.

B. Diffraction Losses

The expressions derived using (3) contain phase information for beam modes traveling between reflectors and thus model the resonance condition. The derived expressions do not include diffraction losses caused by finite reflector aperture sizes which lower the Q of a resonator. Beam modes having higher transverse mode numbers also have energy which is distributed over a relatively larger transverse area. Thus we would expect diffraction to more severely reduce the Q of modes having higher transverse mode numbers. This effect is observed in measurements of experimental cavities. In this subsection the effect of diffraction losses is included in the resonator model.

While Hermite–Gaussian functions are often sufficient approximations to the actual resonator field structure, diffraction calculations require use of a more accurate field representation [15]. Diffraction losses have been found by using Huygen's principle and a Green's function to derive an integral equation which relates the fields at one reflector to the fields at the other reflector. Eigenvalues of this equation represent diffraction loss. Boyd and Gordon [15] have solved the integral equation for a confocal resonator with spherical reflectors. The power loss per transit due to diffraction, α_{mn} is

$$\alpha_{mn}=1-|\chi_m\chi_n|^2=1-\left|\frac{2c}{\pi}R^{(1)}_{0,m}(c,1)R^{(1)}_{0,n}(c,1)\right|^2. \tag{27}$$

Where $R^{(1)}_{0n}$ is the prolate spheroidal radial wave function, and $c=a^2k/D$ for reflectors having radius of curvature $b=D$ and a square aperture of width $2a$. This expression applies only to confocal resonators although Boyd and Gordon suggest how diffraction losses for a nonconfocal resonator can be approximated by using values for the confocal case [15]. The spheroidal wave functions are tabulated only for specific values of the parameter c and cannot easily be determined for arbitrary values of c [23], [24]. For this reason, the eigenvalues χ will be found numerically.

Numerical solution for the eigenvalues is accomplished by reducing the integral equation to a matrix eigenproblem. The fields are evaluated at discrete points on the reflectors and Simpson's rule is used to perform the integration. This is the same method used by Soohoo [20] except that it has been extended to include rectangular apertures, and also allows for $F_x\neq F_y$.

The diffraction losses are included in the model by incorporating them into the reflection coefficient, R_{mn}, of the spherical reflector. An effective reflection coefficient

$$\Gamma_{mn}=|\chi_m\chi_n|R_{mn} \tag{28}$$

is computed and is substituted into (25) in place of R_{mn}. Due to the introduction of Γ_{mn}, the relationship (8) is no longer valid as it applies to a lossless junction. The result (25) is still valid because it depends only upon reflection from the spherical mirror and is independent of T_{mn}.

The resonator model is intended for use in an harmonic balance oscillator program. In this environment, diffraction losses must be calculated for all modes at many different simulation frequencies. Rather than solve the eigenproblem at each frequency (different value of the parameter c), the speed of simulation is increased by modeling the resonator mode electric field transition gain, $|\chi_m\chi_n|$, using

$$|\chi_m\chi_n|=\sqrt{(1-A_m10^{-B_mc_x})(1-A_n10^{-B_nc_y})} \tag{29}$$

where the constants A_n, A_m, B_m, B_n are determined by solving the eigenproblem, and $c_{x,y}=ka^2_{x,y}/2D$, and a is the aperture half-width for the plano-concave resonator.

Conductor losses were also included in the effective reflection coefficient. These were determined by the usual surface resistance calculation. The conductor losses of both reflectors is included in Γ_{mn}.

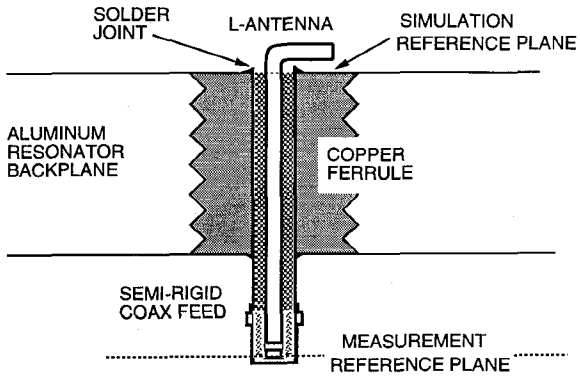

Fig. 4. Geometry of the radiating element.

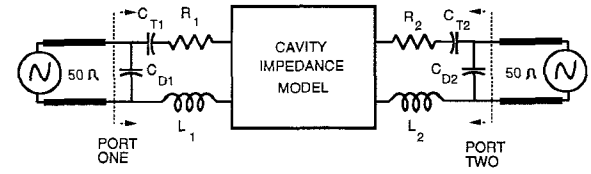

Fig. 5. Two port model for a nonresonant antennas radiating into an open cavity.

V. Computed Results And Experiment

A. Discussion

Here an experimentally measured two port impedance matrix is compared with that predicted by theory. The experimental apparatus consists of a pair of co-axially fed inverted-L antennas [21] radiating into a plano-concave resonator. The geometry of one of the electrically short antennas is represented in Fig. 4. The resonator is similar to that shown if Fig. 1 and is comprised of a planar reflector facing a concave spherical reflector, each fabricated from 6061 T6 aluminum. Measurements were taken using an HP-8510B network analyzer which was calibrated to the plane of the connectors on each antennas' semi-rigid coaxial feed. The simulator model for the antennas and resonator assumes that the reference plane is the inside surface of the planar reflector. For comparison of results, the measured impedances were transformed using the transmission line equation to the same reference plane used by the simulation. The coaxial line was assumed to be lossless.

The model for two short antennas radiating into the resonator is shown in Fig. 5. The cavity impedance model is given by (25) while each electrically short antenna is modeled by a lumped-element circuit. The capacitor C_D represents the discontinuity of the outer conductor of the coaxial line at the simulation reference plane. The open circuited short transmission line formed by the antenna-wire over the ground plane is modeled by C_T. Some energy is lost due to radiation that does not couple into cavity modes, this is represented by R. Although the antenna lengths were about $\lambda/10$ at the frequencies of investigation, resonance phenomena were observed to affect the antenna driving point impedance. So, L was included to account for these effects. Values for these circuit elements were selected by fitting the model to broadband impedance measurements of each antenna over a ground plane.

B. Resonator Characterization

Resonator physical dimensions will be given in terms of λ_{00} which is defined as the free space wavelength associated with $f_{00} = 8.5027$ GHz, the resonant frequency of the $\mathrm{TEM}_{0,0,35}$ resonator mode. The rectangular planar reflector of dimensions $(18.71 \times 18.12)\lambda_{00}$, and the circular sperical reflector of aperture diameter $14.45\lambda_{00}$ were separated by a distance $17.59\lambda_{00}$. This spacing corresponds to approximately $2/3$ of the semiconfocal spacing for the $51.83\lambda_{00}$ radius of curvature spherical reflector. This plano-concave resonator with reflector spacing D is similar to a resonator having two identical spherical reflectors of spacing $2D$ and aperture parameter $c = \pi a^2/D\lambda_{00} = 9.25$.

The physical construction of the resonator should result in Laguerre-Gaussian modes since nearly all diffraction losses occur around the spherical reflector which has a circular aperture. The major diffraction losses occur at the spherical reflector because the beam spot-size is larger on the spherical reflector than it is on the planar reflector and the spherical reflector also has a smaller aperture area. Thus the resulting boundary conditions have cylindrical symmetry, and Laguerre-Gaussian modes are expected. Measurements of the planar reflector show that it is distorted. Along the x-axis the reflector is seen to be concave with a $.0057\lambda_{00}$ dip in $17.27\lambda_{00}$. A convex crown of $.0057\lambda_{00}$ in $8.64\lambda_{00}$ was measured along the y-axis. This distortion has approximate rectangular symmetry and apparently disturbs the resonator cylindrical symmetry producing the experimentally observed Hermite–Gaussian modes. The distortion of the planar reflector was not sufficiently uniform to be characterized through use of mechanical measurements.

The effect of the warped planar reflector on the resonance spectrum can be examined by considering the phase term of (3). At resonance, the phase of a traveling beam mode should be unchanged after one round-trip through the resonator. Thus, if the phase change for a half-trip is $q\pi$, for some integer q, then resonance will occur. These resonant frequencies are then

$$f_{mnq} = \frac{c}{2D}\left[q + \frac{1}{\pi}\left(m+\frac{1}{2}\right)\arctan\sqrt{\frac{D}{2F_x - D}} + \frac{1}{\pi}\left(n+\frac{1}{2}\right)\arctan\sqrt{\frac{D}{2F_y - D}}\right], \quad (30)$$

where c is the speed of light and q, the longitudinal mode number corresponds to an integer number of longitudinal half waves.

Equation (30) predicts families of resonances with each family corresponding to a particular q and having members consisting of resonances with different transverse mode numbers. Each family is offset from the next by $\Delta f = c/(2D)$. Within each family the value of Q decreases quickly for higher mode numbers due to increasing diffraction losses which result from the increase in spot size with increasing transverse mode number. If $F_x = F_y$, then in each family all modes with $m+n$ equal to a constant are degenerate. Observed resonances for the

experimental cavity did not show this degeneracy. In fact the mode spacing corresponds to a resonator with $F_x = 25.34\lambda_{00}$ and $F_y = 27.01\lambda_{00}$. When compared with the nominal focal length of the spherical reflector, $25.9\lambda_{00}$, we see that the concavity of the planar reflector along the x-axis decreases the effective x focal length of the spherical reflector, while the convex shape along the y-axis increases the effective y focal length. These effective focal lengths are used in simulation, thus the distortion of the planar reflector is modeled by slight changes in curvature of the spherical reflector while assuming that the planar reflector is ideal.

No provisions were made in the experimental apparatus for precise alignment of the reflectors. We define the z-axis of the resonator to be a line normal to the planar reflector which intersects the center of the face of the spherical reflector. It can be seen that tilting of the mirrors will effect the location of the coordinate system origin, i.e., the z-axis intersection with the face of the planar reflector. Also, since it is the distortion of the planar reflector which causes the rectangular mode structure, the orientation and origin of the transverse axes $(x-y)$ is unknown. The approximate location of the z-axis and the orientation of the transverse axes were determined by measurement. A small sphere of lossy dielectric was positioned in the resonator near the planar reflector, then the reflection coefficient at an antenna was observed while the sphere was moved. The positions of field nulls for several modes were noted, from this the approximate alignment of the resonator coordinate system was determined. This coordinate system is used to describe the antenna locations during simulation.

Examination of cavity measurements showed that conductor losses were higher than those predicted by surface resistance calculations using bulk conductivity for 6061 T6 aluminum. It is expected that the oxide layer, surface roughness and contamination would increase the value of surface resistance above its ideal value. A constant value for conductor losses was selected based upon examination of data and was used during simulation. A reflection coefficient due to conductor losses of -0.9992 was used rather than the theoretical value of -0.9996 at 8.5 GHz which is for two bounces (once on the spherical reflector and once on the planar reflector).

C. Two Port Experiment Results

For each q, the transverse electromagnetic modes; TEM_{00}, TEM_{10}, TEM_{20}, TEM_{02}, and TEM_{11} were observed. The response for higher transverse mode numbers was very small due to diffraction losses. Two port measurements were made for each of these modes for the $q = 35$ family and are compared with simulated results in Figs. 6–14. The inverted-L antennas for port-1 and port-2 were located at $\{x, y\} = \{-9.06\text{ cm}, 1.5\text{ cm}\} = \{-2.57, 0.425\}\lambda_{00}$ and $\{x, y\} = \{2.7\text{ cm}, 1.7\text{ cm}\} = \{0.767, 0.482\}\lambda_{00}$ respectively. The modes are of high Q so measurements over three frequency ranges were performed to resolve the resonances. Figs. 6 and 7 show the magnitude and phase of z_{11} for the dominant mode and indicate very good agreement between simulation and measurement. The agreement for the TEM_{00} response of z_{22} was also observed to be very good. The agreement between measured and simulated magnitude and that between measured and simulated phase are similar for all measurements, so magnitude information alone will be presented. Fig. 8 shows very good agreement between measured and simulated values of z_{12} for the TEM_{00} mode.

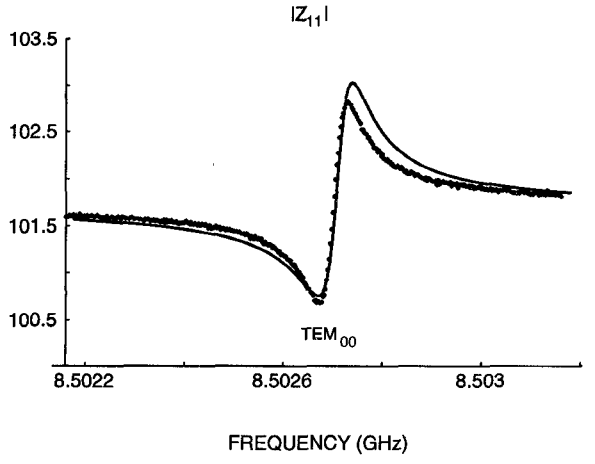

Fig. 6. Measured and simulated values of $|z_{11}|$ for inverted-L antennas in a plano-concave resonator, TEM_{00} mode.

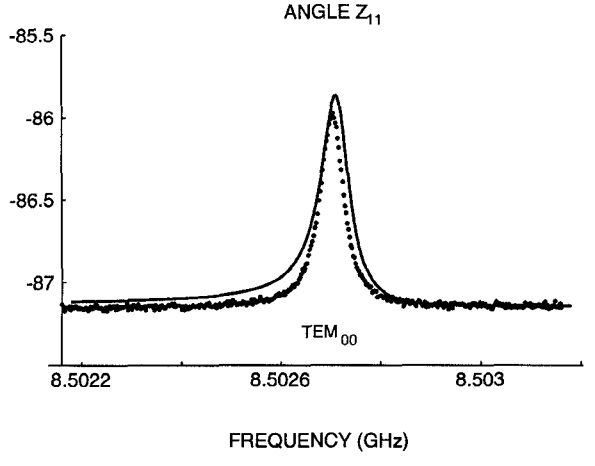

Fig. 7. Measured and simulated values of angle z_{11} for inverted-L antennas in a plano-concave resonator, TEM_{00}, mode.

A comparison for the TEM_{01} and TEM_{10} modes is made in Figs. 9–11. The measured and simulated responses for z_{11} differ by an impedance which is approximately constant over the frequency range shown in this figure. This difference is caused by a systematic measurement error. During calibration of the HP-8510B, calibration standards with 3.5 mm connectors are placed at the measurement reference plane. After calibration, the HP-8510B ports are connected to the antenna feeds which are SMA connectors on RG-402 semirigid coaxial line and reflections occur at this connection. The measurement data is then transformed using the transmission line equation to the simulation plane. This transformed impedance data contains a small periodic ripple whose period corresponds to the length of the antenna feed line and is caused by an interaction between the reflection at the connector, and the transmission line transformation. As a result, the simulated antenna char-

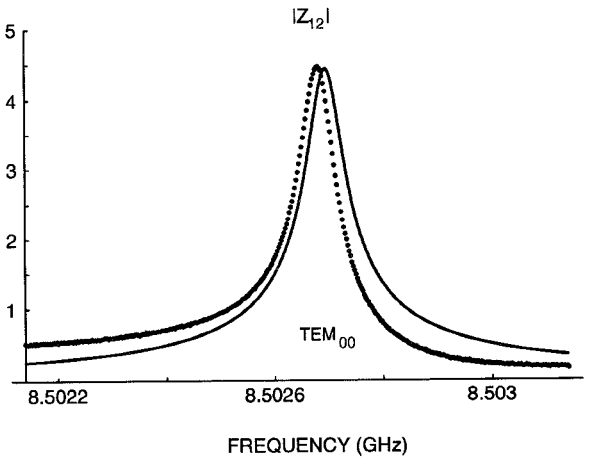

Fig. 8. Measured and simulated values of $|z_{12}|$ for inverted-L antennas in a plano-concave resonator, TEM_{00} mode.

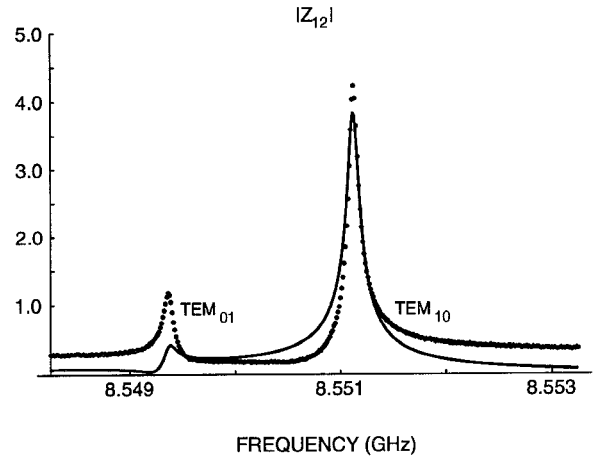

Fig. 11. Measured and simulated values of $|z_{12}|$ for inverted-L antennas in a plano-concave resonator, modes TEM_{01}, TEM_{10}.

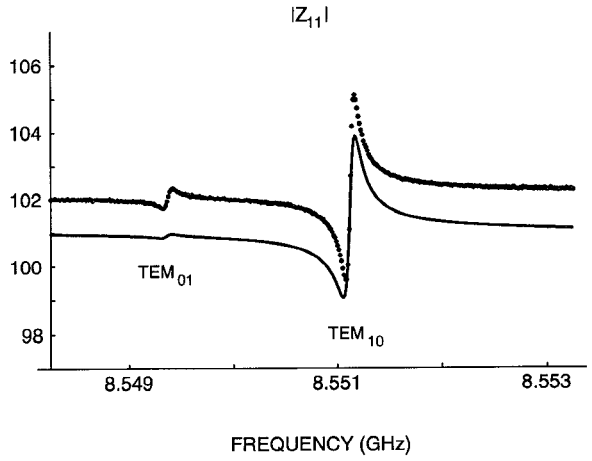

Fig. 9. Measured and simulated values of $|z_{11}|$ for inverted-L antennas in a plano-concave resonator, modes TEM_{01}, TEM_{10}.

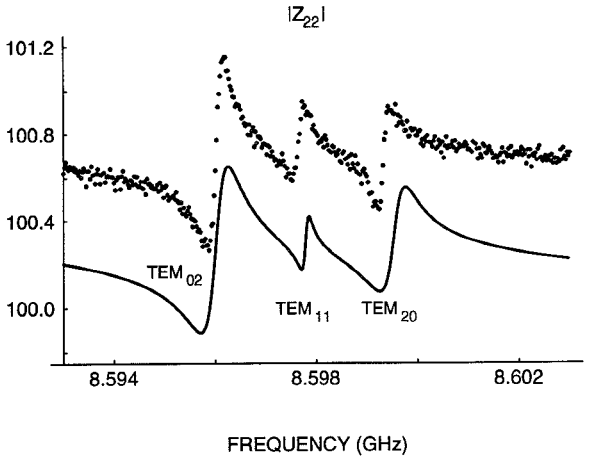

Fig. 12. Measured and simulated values of $|z_{11}|$ for inverted-L antennas in a plano-concave resonator, modes TEM_{02}, TEM_{11}, TEM_{20}.

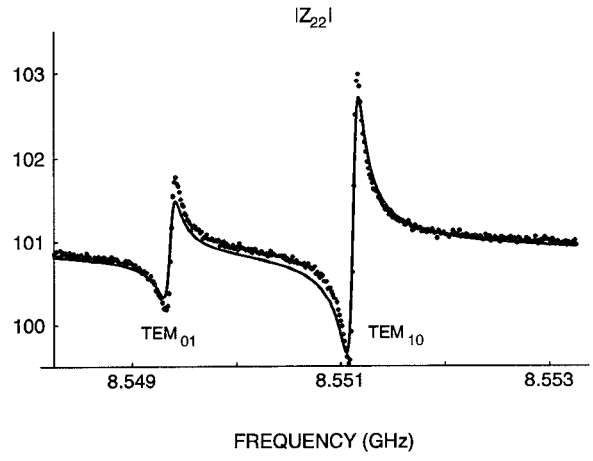

Fig. 10. Measured and simulated values of $|z_{22}|$ for inverted-L antennas in a plano-concave resonator, modes TEM_{01}, TEM_{10}.

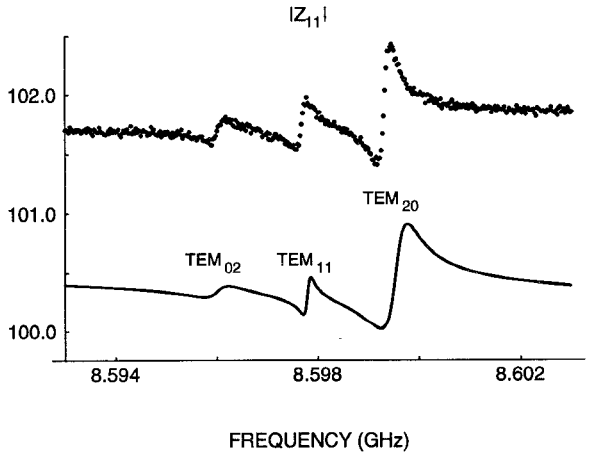

Fig. 13. Measured and simulated values of $|z_{22}|$ for inverted-L antennas in a plano-concave resonator, modes TEM_{02}, TEM_{11}, TEM_{20}.

acteristics differ slightly from those of the physical data for some frequency ranges. Similar impedance offsets are seen in Figs. 12 and 13.

In Fig. 9 we can see that the simulated TEM_{01} mode response is much smaller than the measured response. This is thought to be due to an error in precisely locating the resonator axes during characterization of the resonator. Consequently

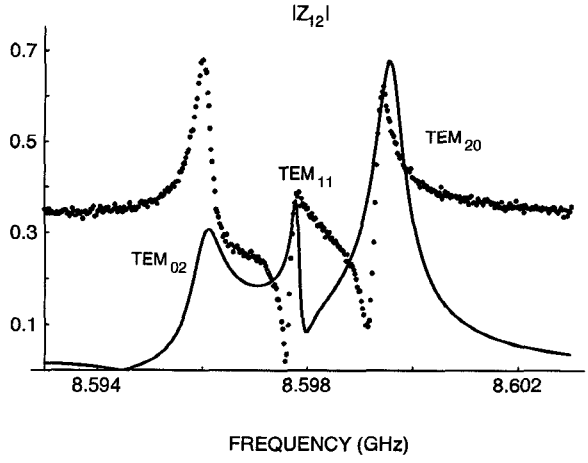

Fig. 14. Measured and simulated values of $|z_{12}|$ for inverted-L antennas in a plano-concave resonator, modes TEM_{02}, TEM_{11}, TEM_{20}.

the simulated antenna location is different from the exact location of the physical antenna. In Fig. 11 it is apparent that the simulated value of $|z_{12}|$ is also affected for the TEM_{01} mode. Another discrepancy is that the simulated value of z_{12} goes to zero at frequencies which are far removed from resonance while the measured value approaches a small nonzero impedance. It is believed that this is due to direct radiation coupling between the two antennas. Direct coupling effects are not presently included in the simulator model.

A comparison of the TEM_{02}, TEM_{11}, and TEM_{20} modes is shown in Fig. 12–14. Again the simulated values for z_{11} and z_{22} are in excellent agreement. In Fig. 14 the coupling through direct radiation is no longer small compared with the coupling though the resonator modes. At some frequencies the two forms of coupling are in phase and reinforce each other, while they are out of phase and apparently of equal magnitude at others.

VI. Conclusion

The impedance matrix for an array of small antennas radiating into a plano-concave quasi-optical resonator has been modeled. The model includes the effects of diffraction loss, and conductor loss, as well as output power coupling and is valid for arbitrary reflector spacing, and arbitrary source location and frequency. This model is suitable for use in a circuit simulator and is intended for use in the design of cavity type quasi-optical power combiners. Very good agreement is shown between simulation and measurement for two inverted-L antennas radiating into a plano-concave resonator. The effects of direct radiation coupling are not included in the model, but are detectable during measurement. In an operating RC power combiner the antennas will have a spacing smaller than that which was used for these two port measurement and there also will be many antennas distributed throughout a transverse plane. The first factor will increase the relative level of direct radiation coupling, the second may decrease it because the direct radiation from the multiple sources will arrive out of phase.

Better agreement is expected if the cavity reflectors are precisely aligned. Although the offset of the cavity axes due to reflector tilting was accounted for in describing antenna locations, it was not used in diffraction calculations. In the derivation of the impedance model, the short antenna approximation was used to evaluate (19) and (21). The input impedance of larger antennas can be calculated using (26). Evaluation of the integrals requires that the antenna current densities be known. The problem can be solved iteratively by assuming no radiation, then expanding the antenna current density in terms of the antenna eigenfunctions. The cavity response is then calculated using (19) and the computed antenna current density. Stored and dissipated power for the cavity are computed, then used to modify the Q of the antenna model. A new antenna eigenfunction expansion is then performed. This procedure is iterated until a self-consistent solution is determined. This method is similar to the cavity model used for patch antennas [22].

References

[1] J. Birkeland and T. Itoh, "Spatial power combining using push-pull FET oscillators with microstrip patch resonators," *1990 MTT-S Dig.*, pp. 1217–1220.
[2] N. Camilleri and B. Bayraktaroglu, "Monolithic millimeter-wave IMPATT oscillator and active antenna," *IEEE Trans. Microwave Theory Tech.*, vol. 36, no. 12, pp. 1670–1676, Dec. 1988.
[3] A. Mortazawi and T. Itoh, "A periodic second harmonic spatial power combining oscillator," *1990 IEEE MTT-S Dig.*, pp. 1213–1216.
[4] J. Birkeland and T. Itoh, "Two-port FET oscillators with applications to active arrays," *IEEE Microwave Guided Wave Lett.*, vol. 1, no. 5, pp. 112–113, May 1991.
[5] R. A. York and R. C. Compton, "Quasi-optical power combining using mutually synchronized oscillator arrays," *IEEE Trans. Microwave Theory Tech.*, vol. 39, no. 6, pp. 1000–1009, June 1991.
[6] Z. B. Popovic, R. M. Weikle II, M. Kim and D. B. Rutledge, "A 100-MESFET planar grid oscillator," *IEEE Trans. Microwave Theory Tech.*, vol. 39, no. 2, Feb. 1991.
[7] J. W. Mink, "Quasi-optical power combining of solid-state millimeter-wave sources," *IEEE Trans. Microwave Theory Tech.*, vol. 34, Feb. 1986, pp. 273–279.
[8] C. Xue and Q. Wang, "Discussion of the source-array plane location in the quasi-optical cavity for solid state power combining," *Int. J. Infrared and Millimeter Waves*, vol. 9, no. 8, pp. 725–731, 1988.
[9] Q. Wang, C. Xue, H. Li, and F. Wu, "Optimized design of quasi-optical source-array of solid state power combiner at frequency 100 GHz," *Int. J. Infrared and Millimeter Waves*, vol. 11, no. 11, pp. 1269–1283, 1990.
[10] G. D. Boyd and H. Kogelnik, "Generalized confocal resonator theory," *Bell Syst. Tech. J.*, July 1962, pp. 1347–1369.
[11] A. G. Fox and T. Li, "Resonant modes in a maser interferometer," *Bell Syst. Tech. J.*, Mar. 1961, pp. 453–489.
[12] R. W. Zimmerer *et al.*, "Millimeter wavelength resonant structures," *IEEE Trans. Microwave Theory Tech.*, Mar. 1962, pp. 142–149.
[13] R. W. Zimmerer, "Spherical mirror Fabry–Perot resonators," *IEEE Trans. Microwave Theory Tech.*, Sept. 1963, pp. 371–379.
[14] A. G. Fox and T. Li, "Modes in a maser interferometer with curved and tilted mirrors," *Proc. IEEE*, Jan. 1963, pp. 80–89.
[15] G. D. Boyd and J. P. Gordon, "Confocal multimode resonator theory for millimeter through optical wavelength masers," *Bell Syst. Tech. J.*, Mar. 1961, pp. 489–509.
[16] G. Goubau, "Beam waveguides," in *Advances in Microwaves*, vol. 3, New York: Academic Press, 1968, pp. 67–126.
[17] G. Goubau and F. Schwering, "On the guided propagation of electromagnetic wave beams," *IRE Trans. on Antennas and Propagat.*, May 1961, pp. 248–256.
[18] R. E. Collin, *Foundations for Microwave Engineering.* New York: McGraw-Hill, 1966.
[19] C. A. Balanis, *Antenna Theory, Analysis and Design.* New York: Harper and Row, 1982.
[20] R. F. Soohoo, "Nonconfocal multimode resonators for masers," *Proc. IEEE*, Jan. 1963, pp. 70–75.
[21] K. Fujimoto, A. Henderson, K. Hirasawa, and J. R. James, *Small Antennas*, Research Studies Press LTD, 1987.
[22] K. Chang, *Handbook of Microwave and Optical Components*, vol. 3, New York: Wiley, 1990, pp. 173.

[23] Flammer, *Spheroidal Wave Functions,* Stanford University Press, 1957.
[24] Stratton, Morse, Chu, Little and Corbato, *Spheroidal Wave Functions,* New York: Wiley, 1956.

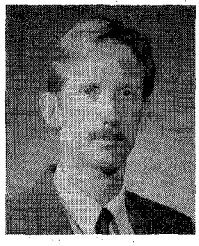

Patrick L. Heron received the B.S.E.E. degree in 1983 from California State University Sacramento, the M.S.E.E. degree from University of Central Florida in 1987, and the Ph.D. in Electrical Engineering from North Caroline State University in 1993.

From 1983 to 1987 he taught the Physics, Electrical Engineering, and Controls subjects at the United States Naval Nuclear Power School in Orlando, Florida. His research interests include microwave and analog circuits, electromagnetics, and simulation of high speed circuits. Dr. Heron is presently employed at Geophex, Ltd. in Raleigh, NC where he conducts rsearch and development for instrumentation used in geophysical exploration.

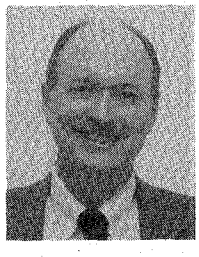

Gregory P. Monahan received the B.S.E.E. from the University of Maryland, College Park in 1967 and the M.E.E.E. from the University of Virginia, Charlottesville in 1989.

From 1967 to 1971 he worked for the U.S. Naval Oceanographic Office, Instrumentation Division in the areas of electronic navigation and data acquisition. From 1971 to 1986 he worked in the construction industry beginning as a carpenter and culminating in managing his own general contracting construction company in Rappahannock County, Virginia. From 1983 to 1986 he was a business manager for Wakefield School, a K-12 private school in rural Virginia. He is currently working towards his Ph.D. degree in Electrical Engineering at North Caroline State University in the Area of microwave and millimeter wave quasi-optical power combining. His research interests are electromagnetics and microwave circuits.

Mr. Monahan is a student member of the Institute for Electrical Engineers and Electronics and a student member of the American Society for Engineering Education.

J. W. Mink (S'59–M'65–SM'81–F'91) for photograph and biography see this issue, p. 1662.

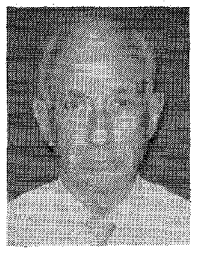

Felix K. Schwering was born on June 4, 1930, in Cologne, Germany. He received the Dipl. Ing. degree in electrical engineering and the Ph.D. degree from the Technical University of Aachen, West Germany, in 1954 and 1957, respectively.

From 1956 to 1958, he was Assistant Professor at the Technical University of Aachen. In 1958 he joined the U.S. Army Research and Development Laboratory at Fort Monmouth, NJ, where he performed basic research in free space and guided propagation of electromagnetic waves. From 1961 to 1964 he worked as a member of the research staff of the Telefunken Company, Ulm, West Germany, on radar propagation studies and missile electronics. In 1964 he returned to the U.S. Army Electronics Command, Fort Monmouth, NJ, (now CECOM), and has since been active in the fields of antennas, wave propagation, random media, and electromagnetic theory in general. Recently he has been involved in particular, in mm-wave antenna and propagation studies. Since 1990 he holds a second (part-time-position as a Visiting Laboratory Scientist at the U.S. Army Research Office, Research Triangle Park, NC.

Dr. Schwering is a Fellow of the IEEE. He is a Visiting Professor at New Jersey Institute of Technology and a member of URSI, Commission B. He received the 1961 and 1982 Best Paper Awards of the IEEE Antennas and Propagation Society (jointly with G. Goubau), and from 1987 to 1989 served as a Distinguished Lecturer of this society.

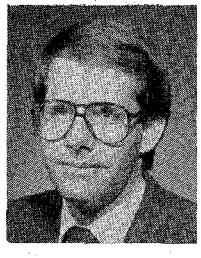

Michael B. Steer received his B.E. and Ph.D. in Electrical Engineering from the University of Queensland, Brisbane, Australia, in 1978 and 1983 respectively. Currently he is director of the Picosecond Digital Systems Laboratory (PICOLAB), co-director of the High Frequency Electronics Laboratory, and Associate Professor of Electrical and Computer Engineering at North Caroline State University.

One aspect of his research involves the experimental characterization, simulation, and computer aided design of high speed digital systems including interconnect simulation, the behavioral model development of digital drivers and receivers incorporating simultaneous switching noise, and the characterization of multichip modules. His continuing interests are in the simulation and modeling of advanced packaging, and in the computer aided analysis and design of nonlinear microwave circuits and systems, with contributions in steady-state simulation of microwave analog circuits, parameter extraction using simulated annealing techniques, microwave measurements, and simulation of millimeter-wave quasi-optical power combining systems. The power combining work includes field-theoretic modeling of quasi-optical systems and transient simulation of power combiners with multiple coupled oscillators. He has authored or coauthored more than 80 papers on these topics.

Dr. Steer is a senior member of the Institute of Electrical and Electronic Engineers and is active in the Microwave Theory and Techniques (MTT) Society and the Components Hybrids and Manufacturing Technology (CHMT) Society. In the MTT Society he serves on the technical committees on Field Theory and on Computer Aided Design. In the CHMT Society he serves on the technical program committee on simulation and modeling of packaging for the Electronics Components and Technology Conference.